Characterization of Human Body Shadowing in Measured Millimeter-wave Indoor Channels

Mbugua, Allan Wainaina; Kentaro, Saito ; Zhang, Fengchun; Fan, Wei

Published in:
2018 IEEE 29th Annual International Symposium on Personal, Indoor and Mobile Radio Communications (PIMRC)

DOI (link to publication from Publisher):
10.1109/PIMRC.2018.8580904

Publication date:
2018

Characterization of Human Body Shadowing in Measured Millimeter-wave Indoor Channels

Allan Wainaina Mbugua*, Kentaro Saito†, Fengchun Zhang* and Wei Fan*
*Antennas, Propagation and Millimetre-Wave Systems Section, Department of Electronic Systems
Aalborg University,Aalborg 9220, Denmark
Email: {awm,fz,wfa}@es.aau.dk
†School of Environment and Society, Tokyo Institute of Technology, Tokyo, Japan
Email: {saitouken}@tse.ens.titech.ac.jp

***Abstract*—In this paper, the human shadowing effect is studied at the millimeter-wave band centered at 28 GHz. The analysis takes a holistic view of the opportunities and challenges that are brought by the presence of a human in the millimeter-wave channel. The impact of human body shadowing on the antenna array performance is investigated, where the impairments due to the non-stationarity over the antenna array caused by human-induced shadowing are presented. The spatial-delay information is obtained using a frequency-invariant beamforming algorithm. The measured channel in a free space scenario is compared with the channel when a human subject and a metallic cylinder of similar size to the human subject are present in the channel. The results show that despite a high shadowing attenuation when the human blocks the propagation paths, there are opportunities presented by the presence of the human which can enhance the spatial diversity of the channel at some spatial locations.**

I. Introduction

A judicious study of millimeter-wave (mm-wave) channels is vital for successful deployment of the fifth generation (5G) mobile network. The propagation channel at mm-wave frequencies has substantial differences compared to the channels at sub-6 GHz frequencies where legacy cellular networks operate, with the former exhibiting a higher free space path loss, sparsity and directivity [1]–[3]. Although the free space propagation loss at mm-wave bands is higher, it has been demonstrated that with antenna array gains this propagation loss can be combated owing to the fact that electrically large antenna arrays can be implemented in a compact area as the wavelength is small at mm-wave frequencies [4]. Channel sparsity at mm-wave bands implies that there is a higher probability of signal to noise ratio (SNR) degradation due to blockage of the line-of-sight (LOS) component or the significant multipath components (MPC)s.

Much of the effort reported in literature has focused on the modeling of the human blockage where the human body is treated as a blocking screen and directional antennas have been used in the measurement [5], [6]. The information from these techniques enable the calibration of ray-tracing tools which are used to simulate the impairments to the propagation channel due to human body shadowing [7]. In the METIS channel model, the shadowing attenuation is described in terms of the knife-edge diffraction (KED) [8], [9]. Although KED is an effective way of characterizing and modeling the shadowing attenuation and diffraction for a specific link which in most cases is the LOS component, it does not give a holistic view of the impact the shadowing brought by the human on the propagation channel, since the directive horn antennas used in the measurements in [5], [6] act as spatial filters for the MPCs [10].

In this paper, we begin by recording the channel impulse response (CIR) in a free space scenario which we use as the reference for the analysis. The channel is modified by the introduction of a human subject and the body shadowing effect due to the human is investigated by comparing the CIR with the reference CIR. The analysis is then repeated with a metallic cylinder of similar dimensions as the human subject. A selected number of points are used in the analysis with the consideration that, although human behavior and movement in a channel are rather stochastic, in typical indoor scenarios human location is largely governed by the furniture setting [11]. We simplify the problem further by considering a static channel. The power angle delay profile (PADP) is then obtained using the frequency invariant beamforming (FIBF) algorithm [12]. This FIBF algorithm generates a narrow main beam width and works well in practical 3-D propagation scenarios unlike convectional frequency invariant beamformers that only work for ideal 2-D scenarios. Moreover, the FIBF algorithm does not have joint sidelobes in angle and delay domain like the classical beamformer algorithm [1].

II. Measurement Setup

A. Measurement System

In this measurement campaign, the measurement system utilized is outlined in [13]. The measurement system alleviates the high signal loss at mm-wave frequencies in the coaxial cable by downconverting the radio frequency (RF) signal at the receiver (Rx) antenna to an intermedi-

978-1-5386-6009-6/18/$31.00 ©2018 IEEE

ate frequency (IF) signal. The local oscillator (LO) signal is operated at 1/3 of the frequency of the RF signal. Thus, the signal loss in the coaxial cables is substantially reduced by a factor of approximately 1 dB/m compared to the case where RF signal is propagating in the coaxial cable.

B. Measurement Settings

The center frequency chosen is the 28 GHz which is a candidate band for the 5G cellular network. A bandwidth of 2 GHz enables a delay resolution of 0.5 ns. The number of frequency points is set to 750 and the IF bandwidth is set to 5 kHz. The transmitter (Tx) power is set to 12 dBm. A virtual uniform circular array (UCA) is used to obtain the spatial channel information and it is composed of 360 virtual antenna elements with a radius of 0.24 m and an inter-element distance of approximately 0.4 λ at 29 GHz, where λ denote the wavelength. The Tx [14] and Rx (A-INFO-SZ-2003000/P) antennas are both vertically polarized biconical antennas with an omnidirectional radiation pattern in the azimuth plane and are placed at a height 1.3 m. The height of 1.3 m above the floor is chosen so as to completely cover the first Fresnel region by the standing human subject and the metallic cylinder. Our analysis is limited to the UCA plane, due to the fact that the UCA element radiation pattern has quite a narrow elevation pattern. The measurement time for each channel snapshot takes approximately 12 minutes.

C. Measurement Scenario

The measurements are conducted in a 7.3 m $\times$ 5.5 m meeting room shown in Fig. 1 and Fig. 2, where half of the walls are made of concrete and the other half are made of plasterboard. The center of the UCA is placed in the geometric center of the room. First a measurement is carried out in an empty room scenario without the presence of the human or metallic cylinder. The measurement is then conducted with a human subject standing on selected points in a circle of radius 0.9 m from the center of the UCA indicated in Fig. 1. A hollow metallic cylinder of height 1.55 m and diameter 0.317 m and a thickness of 1 mm is also placed at the same selected positions as the human subject. The human subject is 1.65 m tall, with a chest size of approximately 0.87 m, and was dressed in a cotton t-shirt and a cotton jumper during the measurement campaign.

D. Measurement Procedure

The measurement begins by recording the channel frequency response in the free space scenario, that is when the human subject or metallic cylinder are not present. The measurement is then conducted with the human subject standing still on selected points on a circle. Next, the channel measurement is then conducted with the metallic cylinder on the same positions as

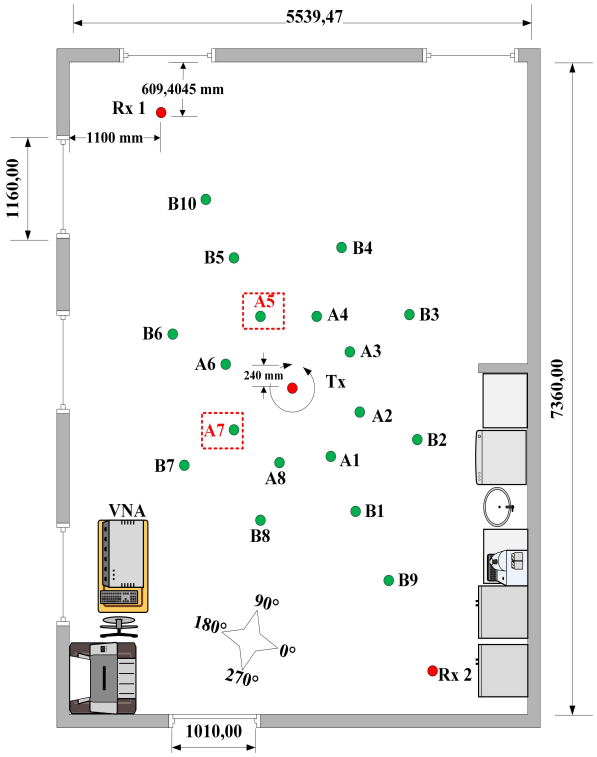

Fig. 1: Measurement scenario and measurement positions. All dimensions are in millimeters.

shown in Fig. 1. Finally the channel is recorded for the free space scenario for verification purposes.

For this analysis we select the spatial positions A5 and A7. At position A5 the human subject and the metallic cylinder create an obstructed-line-of-sight (OLOS) scenario for antenna Rx1. The analysis is repeated for position A7. At position A7 the human subject and the metallic cylinder do not create an OLOS scenario for antenna Rx1 thus this location serves well for a LOS scenario analysis.

III. Signal Model

A UCA of radius r and P omni-directional antenna elements is considered. The location of the *p-th* antenna element can be calculated as:

$$\phi_p = \frac{2\pi \cdot (p-1)}{P} \tag{1}$$

We consider K waves impinging on the UCA, where τ_k and α_k are the delay and the complex amplitude of the *k-th* wave respectively. Taking the center of the UCA as the origin of the coordinate system the channel frequency response at the origin $H(f)$ can thus be obtained as:

$$H(f) = \sum_{k=0}^{K-1} \alpha_k e^{-j2\pi f \tau_k} \tag{2}$$

where f denote the frequency. The channel frequency response at the *p-th* antenna array element $H_p(f)$ is

(a) View from the Rx1 antenna.

(b) Metallic cylinder placed at position A5.

Fig. 2: Measurement scenario photos.

simply a phase shifted version of the array response at the center of the UCA, $H(f)$:

$$H_p(f) = \sum_{k=0}^{K-1} \alpha_k e^{-j2\pi f(\tau_k+\tau_p)} \tag{3}$$

This phase shift comes about due to the propagation delay difference τ_p of the *k-th* wave with azimuth angle of arrival (AOA) φ_k and elevation AOA θ_k, between the *p-th* element and the center of the UCA, which can be obtained as:

$$\tau_p = -\frac{r \cdot \sin(\theta_k) \cdot \cos(\phi_p - \varphi_k)}{c} \tag{4}$$

The antenna array frequency response $H_A(f, \theta, \varphi)$ can be obtained by phase alignment of each of the antenna array element response $H_p(f)$ with the respective complex weight $w_p(f, \theta, \varphi)$.

$$\begin{aligned} H_A(f, \theta, \varphi) &= \sum_{p=1}^{P} w_p(f, \theta, \varphi) \cdot H_p(f) \\ &= \sum_{p=1}^{P} v_p(f, \theta, \varphi) \cdot H(f) \end{aligned} \tag{5}$$

The complex weight $v_p(f, \theta, \varphi)$ can be modified to attain a frequency invariant array beam pattern. This is achieved using the compensation filter $\hat{G}_m(f)$ of the FIBF in [12].

IV. Results

The PADP obtained for the mm-wave channel in the free space scenario is shown in Fig. 3. A 30 dB dynamic range is considered to avoid MPCs close to the noise floor. The channel is composed of several MPCs but only the four dominant MPCs are considered in this analysis. The electrical dimensions of the UCA are relatively

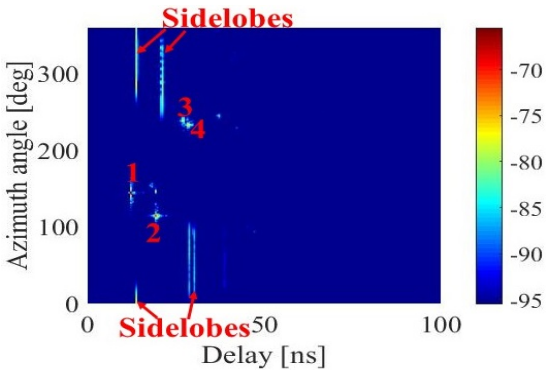

Fig. 3: PADP with the channel in the free space scenario. The color bar represents power in dB.

large, and as can be seen in the power delay profile (PDP) in Fig. 4a, some MPCs exhibit non-stationarity over the array as was also observed in electrically large arrays at sub-6 GHz in [15].

At position A5, the human-induced shadowing attenuation is greater than -30 dB at some antenna element positions of the virtual UCA as shown by path 1 (LOS component) in Fig. 4b causing non-stationarity over the UCA. However, the size of the human subject is small relative to the electrical dimensions of the UCA therefore power is still received by some antenna elements in several spatial locations. Paths 2, 3, and 4 remain unobstructed indicating the possibility of reliable communication even when the LOS component is experiencing human-induced shadowing. Similar results are obtained with the metallic cylinder with the difference being that the shadowing is more severe compared to the human subject.

At position A7 the analysis is carried out of the metallic cylinder instead of the human. The PDP is shown in Fig. 4c where path 3 and 4 are shadowed

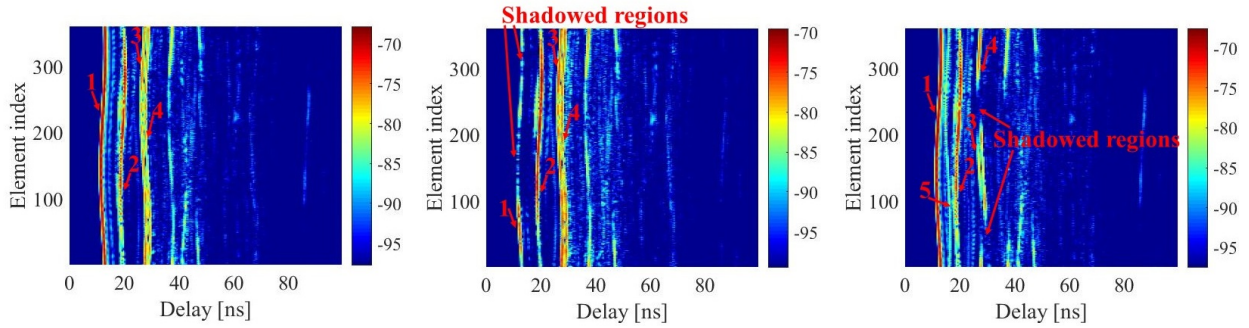

(a) Free space scenario (b) Human at position A5 (c) Metallic cylinder at position A7

Fig. 4: PDP. The color bar represents power in dB.

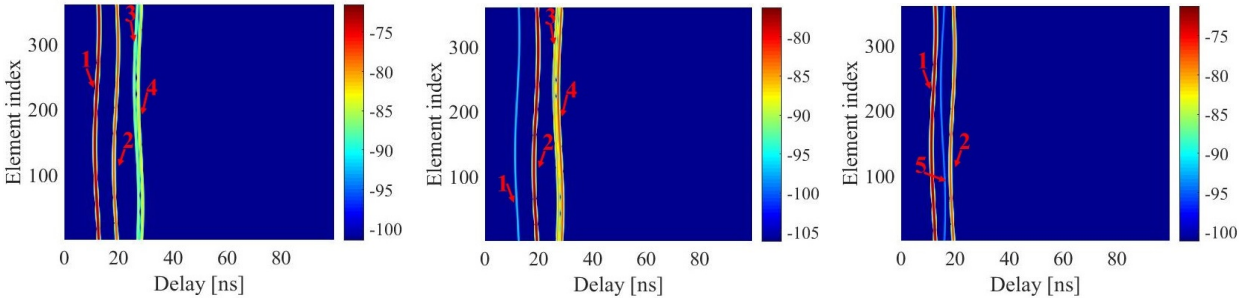

(a) Free space scenario (b) Human at position A5 (c) Metallic cylinder at position A7

Fig. 5: Reconstructed PDP. The color bar represents power in dB.

at some antenna element positions. In this case, path 5 is a reflection from the metallic cylinder. Thus, despite blockage of some paths, new paths are generated. This is also observed when the human is standing at position A7, the difference being that the reflected power from the human is quite low due to differences in the material properties.

The path parameters (τ_k, α_k) identified for the dominant MPCs are picked manually for the reconstruction of the PDP using eq. (3). For the free space scenario the reconstructed PDP from the PADP is shown in Fig. 5a. The stationarity of the four dominant paths over the UCA enable the accurate reconstruction of the PDP in this case.

When the human subject is standing at position A5 the estimated path parameters (τ_k, α_k) from the FIBF lead to an accurate reconstruction of the PDP for path 2, 3 and 4 as shown in Fig. 5b. Path 1 is not reconstructed correctly since the beamforming algorithm assumes stationarity over the array. However, this is not valid anymore as the human subject has caused shadowing over the UCA.

In the third scenario where the metallic cylinder is placed at position A7 the PDP is effectively reconstructed from the path parameters (τ_k, α_k) of the identified paths 1, 2 and 5 as shown in Fig. 5c. Path 3 and 4 are not identified in the AOA estimation due to the non-stationarity over the UCA induced by the shadowing by the metallic cylinder.

A relation of the room trajectory to the identified paths is shown in Fig. 6. Path 1, which is the LOS component, is partially blocked when the human is standing at position A5. The rest of the MPCs are unaffected indicating that with beamforming strategies reliable communication can still be maintained via the MPCs. The significant scatterers in the channel that contribute to the propagation of the MPCs to antenna Rx1 are the concrete wall and the metallic whiteboard.

At position A7 the human subject and the metallic cylinder block paths 3 and 4. This indicates a high probability of outage in a sparse channel and a channel where the significant MPCs originate from closely located spatial locations. However, path 5 can be seen to be generated by the metallic cylinder, showing an opportunity that the obstructors can, in fact, create reliable communication channels.

Path 2 which is a significant MPC with a power level of -71 dB remains unaffected in all the selected points. In fact, as can be observed in Fig. 6, path 2 would still remain unblocked if the human subject was standing in any of the 18 selected positions.

V. Conclusion

The presence of the human in the indoor channel is inevitable as they are the primary users of the 5G

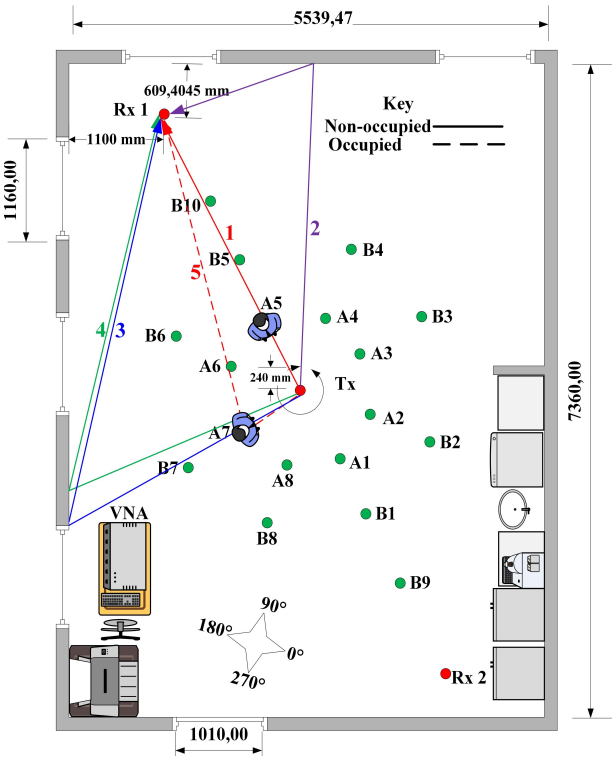

Fig. 6: Path trajectory of the identified paths in relation to the room geometry. The generated paths by the metallic cylinder are shown by the dotted lines. The paths for the free space scenario are indicated by the continuous lines. All dimensions are in millimeters.

network. As demonstrated in the results, the presence of humans in the channel is not all doom and gloom. The physical layer (PHY) design should, in fact, consider exploiting the scattered paths from the human body as a possible propagation path especially in indoor office scenarios where a sedentary lifestyle is common.

The human body shadowing impairments can be overcome for instance by adaptive beamforming techniques where the Tx and Rx can switching to beams that are not in blockage or in a worst case scenario switching to legacy spatial diversity techniques when beamforming is not possible. In the latter case, the antenna array gain is lost, but a communication link can be maintained albeit with reduced performance.

In this analysis, the dimensions of the considered virtual UCA are electrically larger than the human subject. Although this can be a size typical of a base station (BS) antenna array, the 5G mobile station (MS) will have electrically smaller antenna arrays relative to the human body size. It is intuitive to extend this analysis to such scenarios and the inclusion of different human subjects of different body size in a rich multipath environment.

REFERENCES

[1] W. Fan, I. Llorente, J. Nielsen, K. Olesen, and G. Pedersen, "Measured wideband characteristics of indoor channels at centimetric and millimetric bands," *EURASIP Journal on Wireless Communications and Networking*, vol. 2016, no. 58, 2016, special issue on Radio Channel models for higher frequency bands.

[2] J. Medbo, H. Asplund, and J. E. Berg, "60 ghz channel directional characterization using extreme size virtual antenna array," in *2015 IEEE 26th Annual International Symposium on Personal, Indoor, and Mobile Radio Communications (PIMRC)*, 2015, pp. 176–180.

[3] A. W. Mbugua, W. Fan, Y. Ji, and G. F. Pedersen, "Millimeter wave multi-user performance evaluation based on measured channels with virtual antenna array channel sounder," *IEEE Access*, vol. 6, pp. 12 318–12 326, 2018.

[4] B. Ai, K. Guan, R. He, J. Li, G. Li, D. He, Z. Zhong, and K. M. S. Huq, "On indoor millimeter wave massive mimo channels: Measurement and simulation," *IEEE Journal on Selected Areas in Communications*, vol. 35, no. 7, pp. 1678–1690, July 2017.

[5] G. R. MacCartney and T. S. Rappaport, "A flexible millimeter-wave channel sounder with absolute timing," *IEEE Journal on Selected Areas in Communications*, vol. 35, no. 6, pp. 1402–1418, June 2017.

[6] X. Chen, L. Tian, P. Tang, and J. Zhang, "Modelling of human body shadowing based on 28 ghz indoor measurement results," in *2016 IEEE 84th Vehicular Technology Conference (VTC-Fall)*, Sept 2016, pp. 1–5.

[7] V. Degli-Esposti, F. Fuschini, E. M. Vitucci, M. Barbiroli, M. Zoli, L. Tian, X. Yin, D. A. Dupleich, R. Mller, C. Schneider, and R. S. Thom, "Ray-tracing-based mm-wave beamforming assessment," *IEEE Access*, vol. 2, pp. 1314–1325, 2014.

[8] P. Kysti, J. Lehtomki, J. Medbo, and M. Latva-aho, "Map-based channel model for evaluation of 5g wireless communication systems," *IEEE Transactions on Antennas and Propagation*, vol. 65, no. 12, pp. 6491–6504, Dec 2017.

[9] G. R. MacCartney, S. Deng, S. Sun, and T. S. Rappaport, "Millimeter-wave human blockage at 73 ghz with a simple double knife-edge diffraction model and extension for directional antennas," in *2016 IEEE 84th Vehicular Technology Conference (VTC-Fall)*, Sept 2016, pp. 1–6.

[10] M. Jacob, S. Priebe, T. Krner, M. Peter, M. Wisotzki, R. Felbecker, and W. Keusgen, "Fundamental analyses of 60 ghz human blockage," in *2013 7th European Conference on Antennas and Propagation (EuCAP)*, April 2013, pp. 117–121.

[11] S. Obayashi and J. Zander, "A body-shadowing model for indoor radio communication environments," *IEEE Transactions on Antennas and Propagation*, vol. 46, no. 6, pp. 920–927, Jun 1998.

[12] F. Zhang, W. Fan, and G. F. Pedersen, "Frequency-invariant uniform circular array for wideband mm-wave channel characterization," *IEEE Antennas and Wireless Propagation Letters*, vol. 16, pp. 641–644, 2017.

[13] J. Hejselbaek, Y. Ji, W. Fan, and G. F. Pedersen, "Channel sounding system for mm-wave bands and characterization of indoor propagation at 28 ghz," *International Journal of Wireless Information Networks*, vol. 24, no. 3, pp. 204–216, Sep 2017. [Online]. Available: https://doi.org/10.1007/s10776-017-0365-0

[14] S. S. Zhekov, A. Tatomirescu, and G. F. Pedersen, "Antenna for ultrawideband channel sounding," *IEEE Antennas and Wireless Propagation Letters*, vol. 16, pp. 692–695, 2017.

[15] S. Payami and F. Tufvesson, "Channel measurements and analysis for very large array systems at 2.6 ghz," in *2012 6th European Conference on Antennas and Propagation (EUCAP)*, March 2012, pp. 433–437.